EUV actinic brightfield mask microscopy for predicting printed defect images

Kenneth Goldberg*[a], Markus P. Benk[a], Antoine Wojdyla[a], Erik Verduijn[b], Obert R. Wood III[b], and Pawitter Mangat[b]

[a]Center for X-ray Optics, Lawrence Berkeley National Laboratory, Berkeley, CA 94720 U.S.A.
[b]GLOBALOUNDRIES, 400 Stonebreak Road, Malta, NY 12020, U.S.A.

ABSTRACT

Improving our collective understanding of extreme ultraviolet (EUV) photomask defects and the imaging properties of available defect imaging tools is essential for improving EUV mask defectivity, defect repair and mitigation, and for high-level strategic decision-making. In this work, we perform a qualitative comparison of twenty-five defects imaged with mask scanning electron microscopy (SEM), EUV actinic mask imaging, and wafer SEM imaging. All but two of the defect locations were first identified by non-actinic mask blank inspection, prior to patterning. The others were identified as repeating defects on the wafer. We find that actinic defect imaging is predictive of the wafer prints, with small-scale features clearly replicated. While some mask defect SEM images match the wafer prints, others print with a larger outline indicating the presence of sub-surface disruptions hidden from the SEM's view. Fourteen other defects were subjected to an aerial image phase measurement method called Fourier Ptychography (FP). Although phase shifts were observed in the larger defects, the smaller defects in the dataset showed no significant phase shifting. We attribute this discrepancy to non-actinic mask blank inspection's limited ability to detect small phase defects under normal operating conditions.

Keywords: extreme ultraviolet, EUV, mask, defects, actinic, wafer SEM, mask SEM, imaging

1. INTRODUCTION

Mask defects, detection and mitigation remain among of the most challenging problems facing the wide-scale adoption of extreme ultraviolet (EUV) lithography for high volume manufacturing. Despite years of work in this area, and recent advances from groups worldwide, the debate regarding the necessity of actinic (EUV-wavelength) inspection and imaging continues to this day. To some extent, widely held opinions in this discussion are based on the fact that actinic tools for finding and imaging defects have not been widely available for research. Creating production-quality actinic tools requires a considerable investment of time, money, and willpower, and must be an ongoing process for EUV to be successfully introduced into commercial manufacturing.

We believe that the unavailability of imaging data from actinic tools can skew opinions within the EUVL community and can affect the current perception of mask defectivity issues. The objective of this work is to create and share detailed, qualitative comparison data from recent experiments conducted to assess the actinic inspection strategy and also to provide needed guidance for the repairability of phase defects, where possible.

2. DATA COLLECTION

In this work, a high-level comparison is made between three types of defect image data: (1) mask scanning electron microscope (SEM), (2) wafer SEM, and (3) actinic imaging. A description of this experiment and some data has been previously shared by the authors, in Ref. 1, by Mangat, *et al.*

Most of the defects were first identified through non-actinic EUV mask-blank inspection conducted on two tools, a Lasertec M1350, and a Siemens DXF40. These tools detect scattering from defect sites and estimate the size and severity of defects from that data. Generally speaking, defects detected in this manner could originate from substrate imperfections (pits, bumps, etc.), from multilayer defects, and from surface particles and contamination. The coordinates of the defects found in this manner were used to locate defects in the subsequent defect-review imaging.

*KAGoldberg@lbl.gov; phone 1 510 495-2261; fax 1 510 486-4550; goldberg.lbl.gov; sharp.lbl.gov

Photomask Technology 2015, edited by Naoya Hayashi, Bryan S. Kasprowicz, Proc. of SPIE
Vol. 9635, 963514 · © 2015 SPIE · CCC code: 0277-786X/15/$18 · doi: 10.1117/12.2196966

The masks were fabricated with large-area, dense-line patterns to reproduce the conditions of arbitrary features and relative positions on top of a variety of defects. Many defects on the patterned mask were analyzed by a KLA Tencor 6xx, (which operates at 193-nm wavelength) and a reticle SEM. The masks were exposed on ASML NXE3100 and 3300 scanners: only the 3100 data is shown in this paper. Wafer SEM review was performed with a KLA Tencor eDR-7100 on bright-field repeater defects detected with a KLA Tencor 2835 (a deep ultraviolet, DUV, imaging tool), and at the locations identified through blank inspection before patterning. Finally, the SHARP Actinic Reticle Review Project (SHARP) EUV microscope[2,3] was used to image the defects, using conditions that emulate the NXE3100 in terms of numerical aperture (0.25 4xNA) and illumination partial coherence. A subset of the defects were also imaged using a special mode of data collection on SHARP called Fourier Ptychography (FP) microscopy,[4] a computational microscopy method that enables the complex field phase and amplitude to be calculated. This technique is useful for uncovering the phase nature of some defects, which could be a significant factor in creating successful repairs.

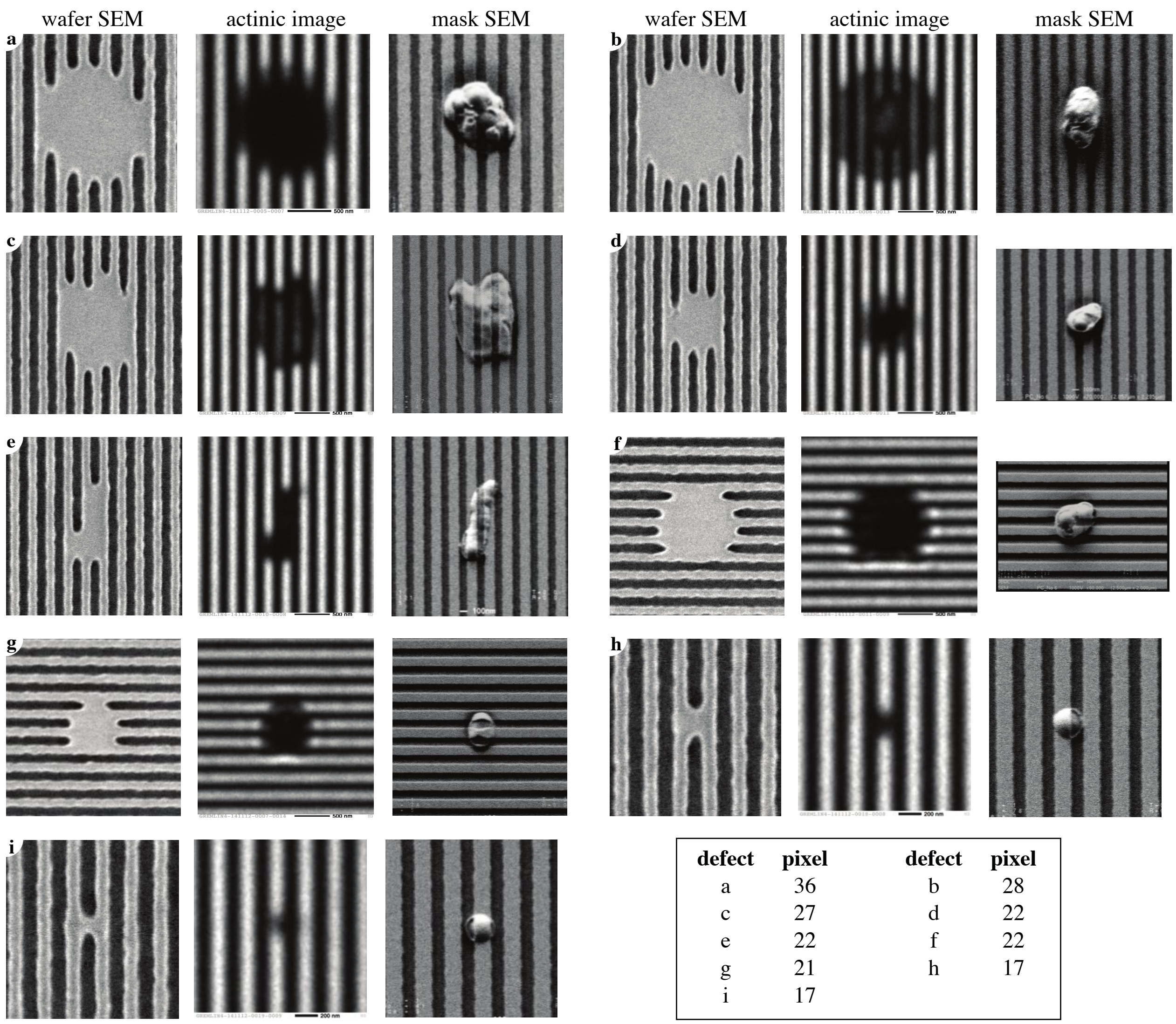

defect	pixel	defect	pixel
a	36	b	28
c	27	d	22
e	22	f	22
g	21	h	17
i	17		

Figure 1. Visual comparison of nine large-sized defects observed with wafer SEM, (EUV) actinic mask imaging, and mask SEM. The images have been scaled and aligned to match. In mask scale, details **a** to **g** are 2-µm wide; **h** and **i** are 1.5-µm wide. The “pixel size” of each defect, as measured by non-actinic blank inspection, is shown in the table.

3. IMAGING COMPARISON

A direct, qualitative comparison of defect images collected with the various imaging modes is presented here. The image details have been scaled, flipped, and aligned to simplify the graphical comparison. The scale of the wafer SEM images (and the features being imaged) is 4× smaller than the mask SEM and the actinic images, owing to the lithography tool's 4× magnification. The image tones are shown in the manner in which they are recorded on each tool. Bright areas in the actinic images represent regions where the local mask reflectivity is high. The actinic images were recorded with a disk-fill profile, using a partial coherence σ value of 0.81.

3.1 Large defects

Figure 1 contains relatively large defects with a strong absorptive character. These are defects assessed by the Lasertec mask blank inspection tool to have "pixel sizes" between 17 and 36. This value represents a categorization system based on the defect's apparent size to the 193-nm illumination. Defect sizes are assessed in this manner before the absorber layer is deposited or patterned.

In all cases shown, the wafer and actinic images appear as faithful visual analogues, and are nominally equivalent. In SHARP, the angular profile of the illumination (i.e. the engineered coherence state) is set to reproduce the conditions used in wafer printing. So the similarity of the two images in these cases validates the predictive quality of the actinic imaging. To produce wafer-equivalent images, a fixed intensity (or dose) threshold would be applied to the continuous tone actinic image, and the scale would be inverted light-to-dark.

Comparison with the mask SEM images shows more subtle effects in play. In some cases, the irregular outline of the defect is clearly observable in the other images. However, in other cases, such as Figs. 1b–e, the printed size of the defect appears to be larger than the disturbance revealed by the mask SEM, and its shape is more circular. This could indicate the presence of sub-surface damage (e.g. substrate bumps or pits) that could disrupt the reflectivity over a somewhat larger area. Interestingly, the actinic image in detail 1b shows visible absorber lines, with reduced amplitude, in the vicinity of the defect. The three-dimensional character or surface profile of these defects is not known at this time.

3.2 Smaller defects

For the defects shown in Figure 2, mask SEM images are not available and the visual comparison is made between the wafer prints and corresponding actinic images. In these cases, the mask blank inspection pixel sizes vary from 1 to 11.

From this series, with smaller defects, we observe that larger pixel size values do not predict the severity of the printed defects. The data show that defects with smaller pixel sizes can induce line bridging (e.g. Fig. 2n); and several defects with the same pixel size (Figs. 2d, e, f, g) can induce substantially different results. This variation could be due to the high sensitivity to the position of the defects relative to the overlaying absorber pattern—an effect that has been predicted[5] and observed.[6–9] It is widely accepted that small defects can be effectively hidden or suppressed below an absorber, yet defects that fall close to the absorber edge may induce increased imaging disruption. Alternately, the actinic magnitude of the defects may not be accurately represented by the reported pixel size. Both of these explanations may be valid, and more work is required to resolve the question. Future experiments should include actinic blank inspection or imaging. These results also indicate the need to classify defects from the mask repair perspective; that would reduce the printable defects at the wafer level and lower the risks for EUV defect printability.

3.3 Pattern defects

Two of the defects shown here are considered to be *pattern defects* because they appear on the mask and in the wafer images, but were not observed during mask blank inspection. Figure 3 shows wafer SEM, actinic image, and mask SEM details of them. Again we see a visual agreement between the wafer SEM and the actinic imaging. However, there are subtle variations observable between the mask SEM and the others, especially in Fig. 3a. Judging by the wafer and actinic images, the extent of the darker region on the mask is somewhat larger than it appears to be from the mask SEM alone. For this reason, the repair of naturally occurring pattern defects could be vulnerable to effects not observable by mask SEM alone. Additional work is required to gather statistical trends on this phenomenon.

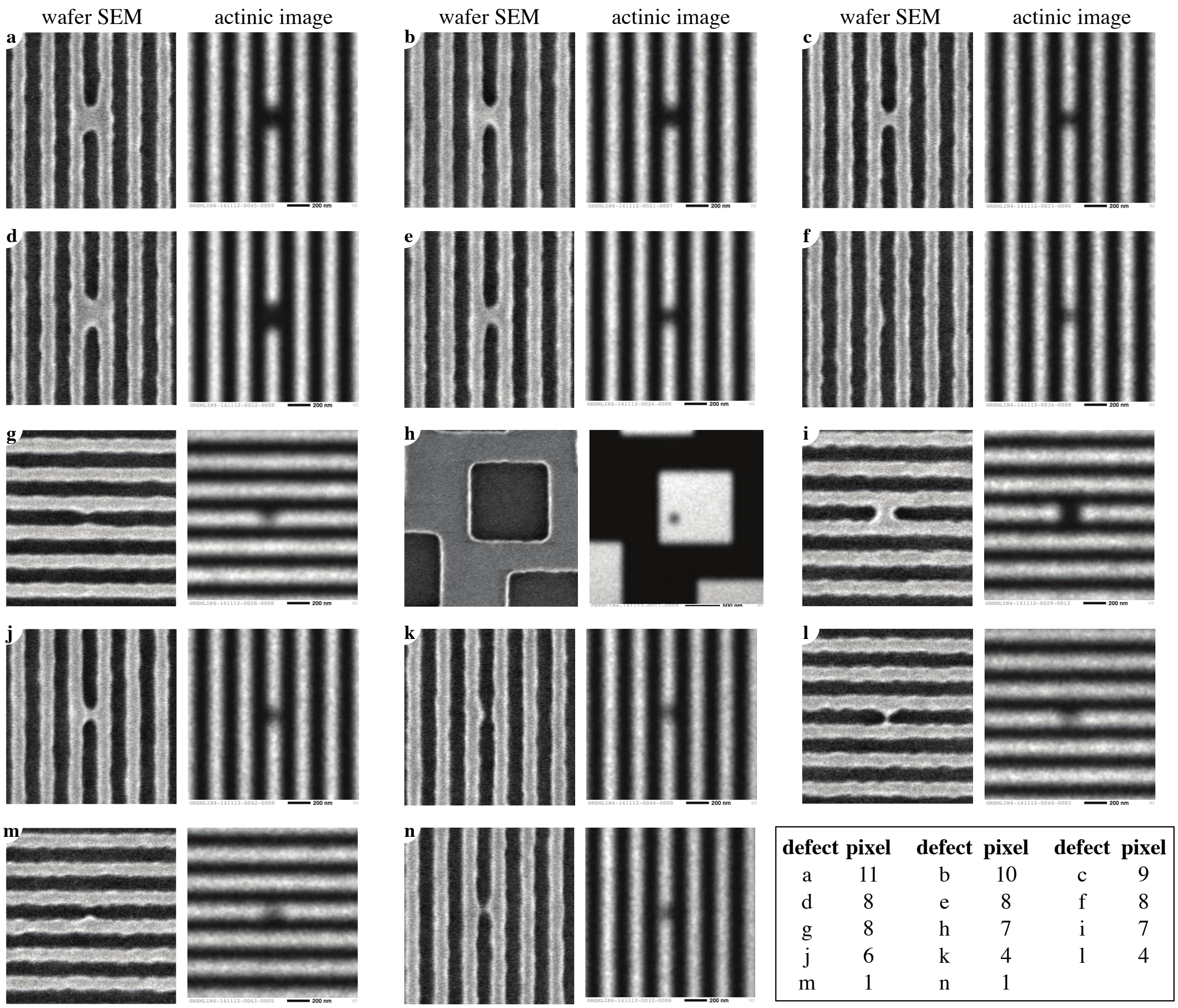

defect	pixel	defect	pixel	defect	pixel
a	11	b	10	c	9
d	8	e	8	f	8
g	8	h	7	i	7
j	6	k	4	l	4
m	1	n	1		

Figure 2. Visual comparison of fourteen small defects observed with wafer SEM and actinic mask imaging. The images have been scaled and aligned to match. In mask scale, details are 1.5-μm wide, except for **h** which is 2-μm wide. The "pixel size" of each defect, as measured by non-actinic blank inspection, is shown in the table. Low defect pixel size does not guarantee a non-bridging defect. Varying behavior from defects of similar size shows that position and other factors may be having a strong influence on defect severity.

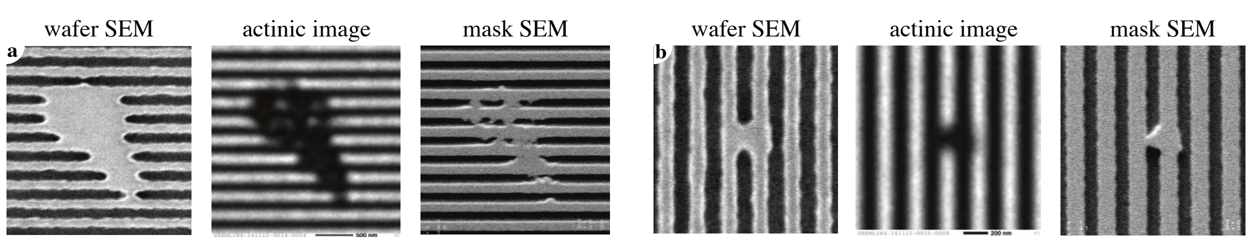

Figure 3. Visual comparison of two pattern defects, observed with wafer SEM, actinic imaging, and mask SEM. In mask scale, detail **a** is 2.5-μm wide, and **b** is 1.5-μm wide.

4. DEFECT PHASE MEASUREMENT

When an image is recorded, whether in photoresist, or with an actinic microscope, only the light intensity is captured, the phase information is "lost." However, the local phase dictates how the light propagates on small and large length scales, and dictates the through-focus behavior to a large extent. Therefore it follows that measuring phase would be an important asset in the successful repair or mitigation of mask defects.

The SHARP microscope and its predecessor, the Actinic Inspection Tool (AIT) have been used to study the phase of defects,[10,11] phase-shifting structures,[12] and image speckle created by mask roughness.[13,14] Previous work used a Gerchberg-Saxton-type reconstruction technique based on a series of images recorded through-focus. More recently, we have been developing an alternative technique based on Fourier Ptychography (FP).[4,15,16] In FP, a series of images are recorded, in-focus, under coherent illumination, varying only the illumination angle for each image. Computation is performed in the Fourier domain where a self-consistent, complex-valued field is synthesized iteratively from the Fourier transforms of the images. The illumination angles are spaced closely enough to provide overlapping data in the Fourier domain for ptychographic reconstruction. The method is robust to noise, and enables the collection of imaging data with higher numerical aperture than the physical lens, due to the aperture synthesis. A more complete description of this technique is now in preparation.

Actinic imaging and FP analysis were performed on fourteen native defects similar to the ones described in Section 3. All of the defects were first identified by non-actinic blank inspection, and their reported pixel sizes range from 1 to 30. Among the five defects with pixel sizes of 17 and higher, all of the defects show phase effects. Phase shifts typically are below $\pi/2$ (90°) in amplitude, relative to the regions adjacent to the defect. Nine smaller defects, with pixel sizes from 1 to 9, show strong amplitude changes, but no significant phase effects.

We see two possible explanations for the lack of phase shifting from smaller defects here. Either small defects have very little phase-shifting nature, or the small phase defects present on the mask escaped detection during inspection with 193-nm light. Authors have previously reported the measurement of small programmed[6,7] and native[17,18] phase defects, showing that pattern replication can be disrupted by defects with 0.5–1.0 nm substrate bump height, and that defects with strong phase can have lateral widths smaller than the imaging resolution. The absence of small phase defects from this, limited dataset, might reveal more about the detection sensitivity under normal working conditions, than about the nature of small defects.

5. CONCLUSION

Despite the well-recognized importance of mask defects as a critical issue for the commercialization of EUV lithography, there is scarce published data comparing mask SEM, actinic imaging, and wafer SEM of known, native defects. In this study, numerous defect locations were identified by mask blank inspection and subjected to study by several techniques.

We observe that actinic imaging, performed with conditions that reproduce lithographic printing, is qualitatively predictive of printing results, down to fine details on a sub-resolution scale. Mask SEM of the smaller defects also predicts the appearance of printed defects, to a large extent. However, several of the defects in this dataset induced larger-area disturbances that the corresponding mask SEM images would suggest. This can be attributed to sub-surface disruptions in the vicinity of the defects that are essentially invisible to the SEM. We also found that blank-defects categorized as having a certain size (by non-actinic blank inspection) can induce a wide range of defect severities. In some cases, defects labeled as "pixel 1" (small) can induce bridging, while larger, "pixel 8" defects can cause little disruption. This observation supports the well-accepted idea that the absorber pattern can either reduce or enhance the printed size of defects, depending on its relative position. Furthermore we note that such defects can be candidates for mask repair by either adding to or shaping the absorber.

Researchers have predicted and shown that defect phase will be an important factor in printability and repair.[7,8,19] Despite this, little published information exists correlating actinically measured defect phases to printability or repair. On SHARP, we observed significant phase effects from several large defects. However, the smaller defects in our dataset show little phase shifting. We believe that small phase defects on the masks may fall below the detection sensitivity used in the non-actinic mask blank inspection that provided the defect locations for this dataset. This conclusion is consistent with prior work based on non-actinic mask inspection and the analysis of repeated defects detected on printed wafers.[20,21]

For greater clarity on this issue, additional investigations are required, focusing on smaller-sized mask defects identified by the inspection of wafer prints.

The investigation of native defects, with side-by-side comparison of the available techniques, can be used to guide defect repair efforts and to inform high-level decision-making about the importance of various tools in the efficient production of patterned EUV masks. Since the predictive ability of actinic imaging tools has been verified, and such tools are either available or are becoming available for research, we recommend that their capabilities should be brought to bear on the challenging problems associated with EUV mask defectivity at current and future EUV technology nodes. Future work should also include defect locations identified by actinic blank inspection, which was not considered in this report.

6. ACKNOWLEDGMENT

This work was funded by GlobalFoundries and SEMATECH. Actinic imaging and analysis was performed by the University of California, Lawrence Berkeley National Laboratory under the auspices of the U.S. Department of Energy, Contract No. DE-AC02-05CH11231. The authors would like to acknowledge the support provided by Advanced Mask Technology Center (AMTC), Dresden, Germany, for patterning the EUV masks and providing optical inspection data for the blank defects.

REFERENCES

[1] Mangat, P., Verduijn, E., Wood, O. R. II, Benk, M. P., Wojdyla, A., Goldberg, K. A., "Mask blank defect printability comparison using optical and SEM mask and wafer inspection and bright field actinic mask imaging," *Proc. SPIE* **9658**, 96580E (2015).

[2] Goldberg, K. A., Mochi, I., Benk, M., Allezy, A. P., Dickinson, M. R., Cork, C. W., Zehm, D., Macdougall, J. B., Anderson, E., Salmassi, F., Chao, W. L., Vytla, V. K., Gullikson, E. M., DePonte, J. C., Jones, M. S., Van Camp, D., Gamsby, J. F., Ghiorso, W. B., Huang, H., Cork, W., Martin, E., Van Every, E., Acome, E., Milanovic, V., Delano, R., Naulleau, P. P., Rekawa, S. B., "Commissioning an EUV mask microscope for lithography generations reaching 8 nm," *Proc. SPIE* **8679**, 867919 (2013).

[3] Goldberg, K. A., Benk, M. P., Wojdyla, A., Mochi, I., Rekawa, S. B., Allezy, A. P., Dickinson, M. R., Cork, C. W., Chao, W., Zehm, D. J., Macdougall, J. B., Naulleau, P. P., Rudack, A., "Actinic mask imaging: Recent results and future directions from the SHARP EUV Microscope," *Proc. SPIE* **9048**, 90480Y (2014).

[4] Zheng, G., Horstmeyer, R. Yang, C., "Wide-field, high-resolution Fourier ptychographic microscopy," *Nature Photonics* **7,** 793 (2013).

[5] Clifford, C. H., Wiraatmadja, S., Chan, T. T., Neureuther, A. R., Goldberg, K. A., Mochi, I., Liang, T., "Comparison of fast three-dimensional simulation and actinic inspection for extreme ultraviolet masks with buried defects and absorber features," *J. Vac. Sci. Technol. B* **27** (6), 2888 (2009).

[6] Huh, S., Kearney, P., Wurm, S., Goodwin, F., Goldberg, K., Mochi, I., Gullikson, E., "Mask Defect Verification Using Actinic Inspection and Defect Mitigation Technology," *Proc. SPIE* **7271,** 72713J (2009).

[7] Huh, S., Kearney, P., Wurm, S., Goodwin, F., Han, H., Goldberg, K., Mochi, I., Gullikson, E., "EUV Actinic Defect Inspection and Defect Printability at the Sub-32 nm Half-pitch," *Proc. SPIE* **7470**, 74700Y (2009).

[8] Kang, I.-Y., Seo, H.-S., Ahn, B.-S., Lee, D.-G., Kim, D., Huh, S., Koh, C.-W., Cha, B., Kim, S.-S., Cho, H.-K., Mochi, I., Goldberg, K. A., "Printability and inspectability study with substrate programmed pit defects in EUV lithography," *Proc. SPIE* **7636**, 76361B (2010).

[9] Kwon, H. J., Harris-Jones, J., Cordes, A., Satake, M., Li, Y., Mochi, I., and Goldberg, K. A., "EUV mask multilayer defects and their printability under different multilayer deposition conditions," *Proc. SPIE* **8322**, 832209 (2012).

[10] Mochi, I., Goldberg, K. A., Xie, R., Yan, P.-Y., Yamazoe, K., "Quantitative evaluation of mask phase defects from through-focus EUV aerial images," *Proc. SPIE* **7969**, 79691X (2011).

[11] Wang, Y.-G., Wojdyla, A., Benk, M. P., Goldberg, K. A., Neureuther, A. R., Naulleau, P. P., Waller, L., "Phase measurements of EUV mask defects," *Proc. SPIE* **9422**, 942217 (2015).

[12] Yan, P.-Y., Mochi, I., Goldberg, K., "EUV Actinic Imaging Tool Aerial Image Evaluation of EUVL Embedded Phase Shift Mask Performance," *Proc. SPIE* **8322**, 83221P (2012).

[13] George, S. A., Naulleau, P. P., Gullikson, E. M., Mochi, I., Salmassi, F., Goldberg, K. A., Anderson, E. H., "Replicated mask surface roughness effects on EUV lithographic patterning and line edge roughness," *Proc. SPIE* **7969**, 79690E (2011).

[14] Naulleau, P., Bhattaria, S., Chao, R., Claus, R., Goldberg, K., Goodwin, F., Gullikson, E., Lee, D., Neureuther, A., Park, J.-J., "Extreme ultraviolet mask roughness: requirements, characterization, and modeling," *Proc. SPIE* **9256**, 92560J (2014).

[15] Tian, L., Li, X., Ramchandran, K., Waller, L., "Multiplexed coded illumination for Fourier Ptychography with an LED array microscope," *Biomed. Opt. Exp.* **5** (7), 2376–89 (2014).

[16] Wojdyla, A., Benk, M. P., Johnson, D. G., Donoghue, A., Goldberg, K. A., "Fourier Ptychography Microscopy with the SHARP EUV Microscope for increased imaging resolution based on illumination diversity," *2014 International Symposium on Extreme Ultraviolet Lithography*, Washington D.C., October 27, 2014.

[17] Gallagher, E., Wagner, A., Lawliss, M., McIntyre, G., Seki, K., Isogawa, T., Nash, S., "Learning from native defects on EUV mask blanks," *Proc. SPIE* **9256**, 92560K (2014).

[18] Terasawa, T., Amano, T., Yamane, T., Watanabe, H., Toyoda, M., Harada, T., Watanabe, T., Kinoshita, H., "At wavelength observation of phase defect embedded in EUV mask using microscope technique," *Proc. SPIE* **9048**, 904825 (2014).

[19] McIntyre, G. R., Gallagher, E. E., Robinson, T. E., Smith, A. C., Lawliss, M., LeClaire, J., Bozak, R., White, R., Archuletta, M., "Through-focus EUV multilayer defect repair with nanomachining," *Proc*. *SPIE* **8679,** 86791I (2013).

[20] Jonckheere, R., Van den Heuvel, D., Bret, T., Hofmann, T., Magana, J., Aharonson, I., Meshulach, D., Hendrickx, E., Ronse, K., "Evidence of printing blank-related defects on EUV masks, missed by blank inspection," *Proc. SPIE* **7985**, 79850W (2011).

[21] Jonckheere, R., Van den Heuvel, D., Bret, T., Hofmann, T., Magana, J., Aharonson, I., Meshulach, D., Hendrickx, E., Ronse, K., "Additional evidence of EUV blank defects first seen by wafer printing," *Proc. SPIE* **8166**, 8166E (2011).